

# Effects of physical forms of Mg/teflon/viton decoys on infrared radiation characteristics

Jun Du\*, Hua Guan\*<sup>†</sup>, and Jie Li\*

\*Nanjing University of Science and Technology 200 N. Xiaolingwei Street, Nanjing 210094, PR China

Phone : +86-18066059126

<sup>†</sup> Corresponding author : guanhua@njust.edu.cn

Received : June 5, 2016 Accepted : November 4, 2016

## Abstract

The study aims to identify the differences in radiation characteristics between sheet-like and column-like Mg/teflon/viton (MTV) infrared decoys. The burning characteristics and infrared radiation characteristics of two types of samples at different diameters were tested with an infrared thermal imager and an OPAG33 Fourier transform infrared remote-sensing spectrometer. Results show that at the same diameter, sheet-like decoys exhibit higher burning rate and burning temperature, lower radiation brightness within 2.5-14.0  $\mu\text{m}$ , and higher far-infrared radiation brightness (63.64-227.11  $\text{W}\cdot\text{m}^{-2}\cdot\text{sr}^{-1}$  higher), when compared with column-like decoys. The spectral radiance of sheet-like decoys are distributed mainly in middle- and far-infrared ranges, while the column-like decoys are mainly distributed in near- and middle-infrared waves. With the same physical form, a larger diameter leads to higher burning rate, higher burning temperature, and higher radiation brightness.

**Keywords** : pyrotechnics, Infrared, MTV, radiation characteristics

## 1. Introduction

The pyrotechnic composition of Mg/teflon/viton (MTV) are widely applied to ignition composition, incendiary bombs, signal bombs, solid rocket propellants, and infrared decoys, mainly due to the high burning temperature, high burning stability, and the ability to produce strong radiation within near- and middle-infrared ranges.<sup>1-4)</sup>

Infrared decoys, including the traditional column-like decoys and new sheet-like decoys, have received extensive attention due to the development of leading techniques. As reported, with metal foil as the base, a layer of combustion ointment is pressed onto its surfaces, which efficiently interferes with infrared and millimeter waves<sup>5)</sup>. Decoys materials with adjustable infrared radiation intensity and wavelength can be prepared by plating a spontaneous combustion coating onto carbon fiber surfaces through steam accumulation<sup>6)</sup>. Natural composites can be prepared by plating an active metal layer onto a tinplate<sup>7)</sup>.

CHEN Ming-hua has found that the infrared radiation intensity of MTV is maximized at a Mg/PTFE mass percentage of 50/50<sup>8)</sup>. So, in this study, MTV infrared decoys, with a Mg/PTFE mass percentage of 50/50, were

coated onto foils to make sheet-like decoys. The differences in the burning characteristics and infrared radiation performance were then comparatively analyzed between sheet-like and traditional column-like MTV infrared decoys. The more matured diameter of, 18 mm and 30 mm, were used to investigate the effects of diameter on the burning and radiation performance.

## 2. Experimental

### 2.1 Main materials

Polytetrafluoroethylene (PTFE, or teflon, 5  $\mu\text{m}$ ) was produced by Shanghai 3F New Materials Co., Ltd. Mg powder (100-200 mesh) was produced by Shanghai Longxin Technology Co., Ltd. Viton fluororubbers were produced by Chenguang Fluororubbers Co., Ltd.

### 2.2 Sample preparation

PTFE and Mg were mixed at a mass ratio of 50 : 50 and then dissolved in acetone containing 10% of Viton. Different masses of the slurries were coated onto 18, 23 or 30 mm diameter tin plates to make sure the natural drying sheet-like samples had the same thickness and density.

Some PTFE and Mg were wet-mixed at the mass ratio

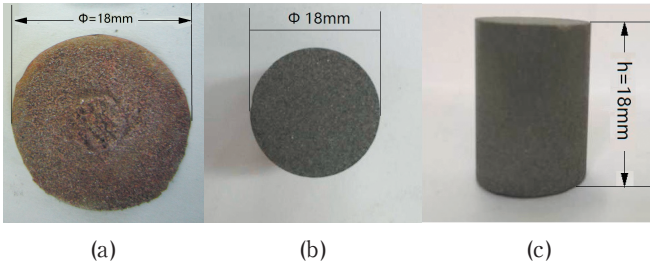


**Figure 1** Schematic of samples. (a) top view of the sheet-like samples; (b) top view of the column-like samples. (c) flat view of the column-like samples

of 50:50 by the acetone containing 10% of Viton, and the humid solid was made into column-like samples at the height about 18mm, the density about  $0.0012 \text{ g}\cdot\text{mm}^{-3}$ , and the diameter of 18, 23 and 30 mm by a certain pressure of the moulds<sup>9</sup>. The samples prepared are illustrated in Figure 1.

## 2.3 Instruments and methods

### 2.3.1 Infrared thermal imager

The burning characteristics and far-infrared radiation performances of the samples were tested using an SC7000 far-infrared thermal imager (US Flir Systems), working at a test distance of 1.4m spectral response range from 7.7 - 9.3  $\mu\text{m}$ ; resolution of  $320 \times 240$  pixels, temperature resolution  $< 20 \text{ mK}$ , the test lens of 25 mm the background or atmospheric temperature of  $20 \text{ }^\circ\text{C}$ , the room temperature of  $25 \text{ }^\circ\text{C}$ , and the radiation brightness of 1.

### 2.3.2 Fourier transform infrared (FTIR) remote-sensing spectrometer

Spectral radiation brightness was measured by an OPAG33 FTIR remote-sensing spectrometer (Bruker Corporation, Germany), which worked at a test distance of 1.6m, spectral range of  $4000 - 400 \text{ cm}^{-1}$ ; resolution of  $4 \text{ cm}^{-1}$ ; sample and background scanning time of 1 s; test results were shown in emission spectrograms.

The measured data were transformed into infrared radiation brightness as follows<sup>10</sup>:

$$R(\nu, T) = [S_{BB}(\nu, T) - S_B(\nu)] / H(\nu, T) \quad (1)$$

$$N(\nu, T) = [S(\nu, T) - S_B(\nu)] / R(\nu) \quad (2)$$

where  $R(\nu, T)$  is the instrument's response function at temperature  $T$  (K);  $S_{BB}(\nu, T)$  is the single beam spectrum (SBS) of an absolute blackbody at  $T$ ;  $S_B(\nu)$  is the background SBS;  $H(\nu, T)$  is the absolute radiation of a theoretical Planck blackbody at  $T$ ;  $N(\nu, T)$  is the final infrared radiation brightness;  $S(\nu, T)$  is the SBS of the sample;  $\nu$  is frequency,  $\text{cm}^{-1}$ .

## 3. Results and discussion

### 3.1 Differences in burning characteristics and far-infrared radiation brightness were compared between sheet-like and column-like MTV infrared decoys

The ignition powder was ignited by a lighter and the samples' burning process was recorded by a camera. As shown in figure 2, the time interval between the two pictures of sheet-like samples and column-like samples were 0.5 s and 6 s respectively.

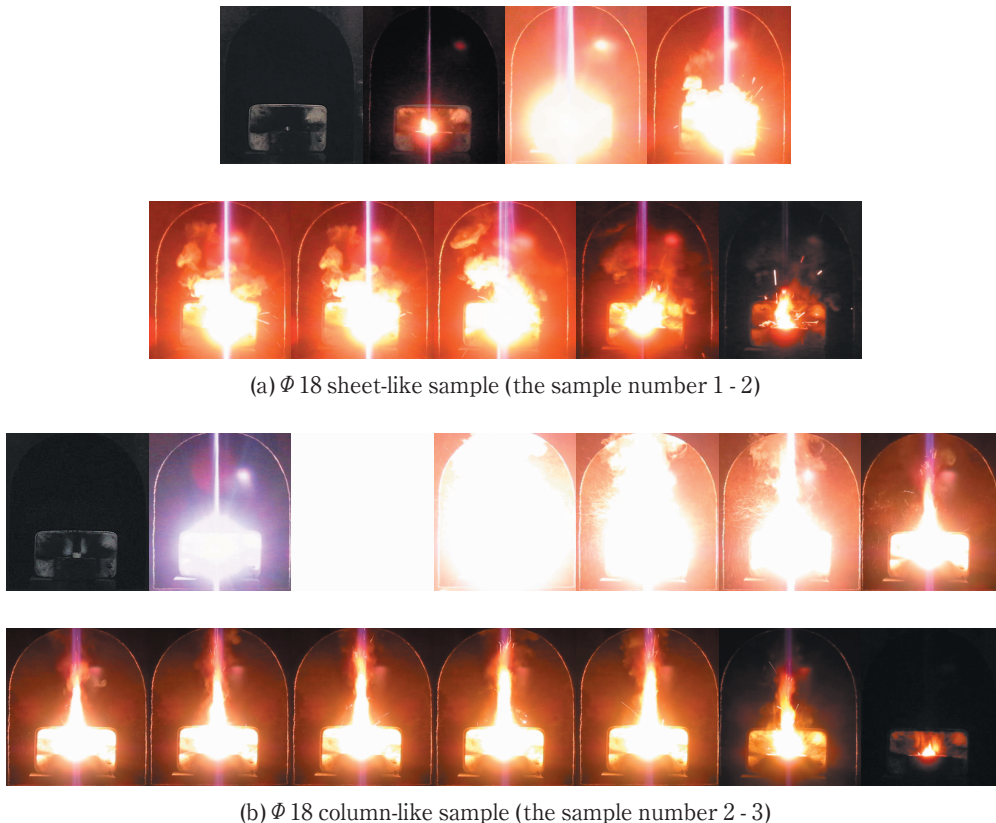


**Figure 2** The burning process  
(the time interval of sheet-like samples is 0.5 s, the time interval of column-like samples is 6 s)

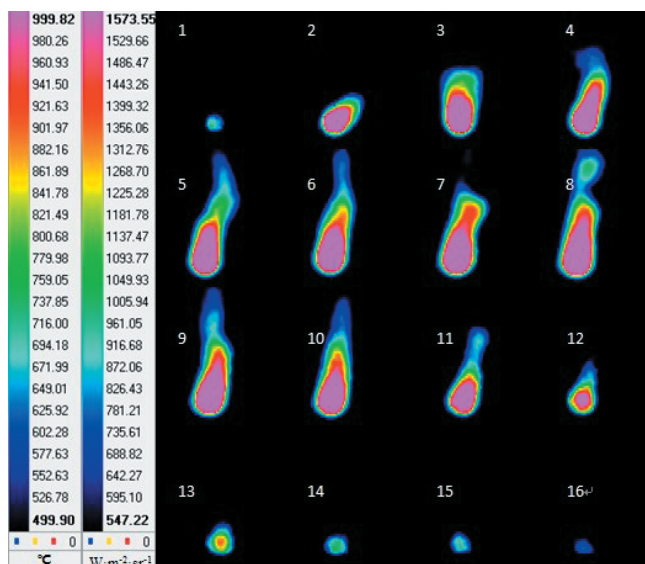


**Figure 3** Infrared thermographs of sheet-like MTV infrared decoys during burning (interval = 0.4 s).

As shown in figure 2, the burning time of column-like samples was much longer than that of sheet-like ones. Also the flames of column-like samples were much bigger and brighter. There was some black solid remainder on the tin plates after burning.

The infrared thermographs illustrating the burning process of decoys were generated by determining the combustion characteristics with the infrared thermal imager. Figure 3 shows the infrared thermographs of sheet-like samples. The built-in infrared thermal imager software, Altair, was used to select the data above 500 °C on all infrared thermographs. Then, the burning time, burning temperature, and radiation brightness during the whole combustion process were computed and expressed in average. Mass burning rate was computed from Equation (3):

$$\dot{m} = M/t \quad (3)$$

where  $M$  is the mass of a sample (g), and  $t$  is the burning time (s).

After many experiments, the average results of burning temperature and far-infrared radiation brightness were listed in Table 1.

As shown in Table 1, when the samples had the same diameters, the sheet-like samples all exhibited higher performance than that of the column-like samples. The burning rate increased by 0.0113 - 0.0269 g·s<sup>-1</sup> (13.7%-31.2%); the burning temperature increased by 11.65-98.84°C (1.1% - 9.0%), and the radiation brightness increased by 63.64-227.11 W·m<sup>-2</sup>·sr<sup>-1</sup> (3.5% - 12.5%). This is because when sample compositions, properties of raw materials, and diameters of samples are all the same, the burning rate of MTV is closely related to its thermal diffusivity. A larger thermal diffusivity means the speeds are higher when all points reach the same temperature, and thus the burning rate is larger<sup>(11), (12)</sup>. Thermal diffusivity  $\alpha$  is expressed as follows:

$$\alpha = \frac{\lambda}{\rho \cdot C_p} \quad (4)$$

where  $\lambda$  is the thermal conductivity,  $\rho$  is the density, and  $C_p$  is the specific heat at a constant pressure.

Then  $\lambda$  and  $C_p$  can be expressed as:

$$\lambda = \frac{\lambda_{Mg} \cdot \lambda_{PTFE}}{\xi_{Mg} \cdot \lambda_{PTFE} + \xi_{PTFE} \cdot \lambda_{Mg}} \quad (5)$$

$$C_p = \xi_{Mg} \cdot C_{pMg} + \xi_{PTFE} \cdot C_{pPTFE} \quad (6)$$

where  $\lambda_{Mg}$  and  $\lambda_{PTFE}$  are the thermal conductivities of Mg and PTFE, respectively;  $\xi_{Mg}$  and  $\xi_{PTFE}$  are the mass percentages of Mg and PTFE, respectively;  $C_{pMg}$  and  $C_{pPTFE}$  are the specific heat capacities at a constant pressure of Mg and PTFE, respectively<sup>(11)</sup>.

As indicated by Equation (5) and (6), both  $\lambda$  and  $C_p$  are the same among all samples. As shown in Table 1, because of the different preparation technologies, the sheet-like samples couldn't be made into those with the density of about 0.0012 g·mm<sup>-3</sup>, also the column-like samples would be powder samples with the density of 0.0008 g·mm<sup>-3</sup>. As for the technological reason, the sheet-like samples have smaller density than column-like samples. So according to Equation (4), sheet-like samples have a higher  $\alpha$ , which means the speed of the heat spreading to the unreacted area is faster. Thus, sheet-like samples show higher burning rate. With the higher burning rate, a larger proportion of compositions is involved in reaction per unit time, indicating larger reaction heat and more energy concentration. Thus, the sheet-like samples have higher burning temperature. The reason is that according to Stefan Boltzmann's law and the law of radiant existence, radiation brightness is in the fourth power of burning temperature, which indicates that infrared radiation brightness is mainly affected by the burning temperature.

As shown in Table 1, contrasting sheet-like or column-like samples only, a larger diameter is associated with higher burning rate, higher burning temperature, and larger far-infrared radiation brightness. Compared with the  $\Phi 18$  samples, the burning rate, burning temperature and radiation brightness of  $\Phi 23$  and  $\Phi 30$  samples increased by 0.0379-0.0784 g·s<sup>-1</sup> (77.5%-130.2%), 33.22-148.82°C (3.0%-14.5%) and 77.07-308.76 W·m<sup>-2</sup>·sr<sup>-1</sup> (4.1%-18.8%) respectively. The burning process of MTV is as follows<sup>(13), (14)</sup>: after being heated, Mg powder particles were fused on the burning surface; then a part of Mg reacted with the F-containing compounds produced from PTFE pyrolysis, while another part entered into the gas phase to undergo rapid oxidation with F. Moreover, the oxidation rate was decided by the concentrations of F and Mg particles both on the burning surface and in the gas phase. Specifically, a higher concentration meant a larger reaction rate, or simply, a higher burning rate. When sample compositions, properties of raw materials, and diameters of samples were all the same, a larger diameter led to the larger burning surface, the concentrations of F and Mg particles on burning surface and in the gas phase were higher, so the reaction rate was larger, there was

**Table 1** Results of burning rate, burning temperature, and far-infrared radiation brightness.

Diameter [mm]	Physical form	Number	Density [ $\text{g}\cdot\text{mm}^{-3}$ ]	Burning rate [ $\text{g}\cdot\text{s}^{-1}$ ]	Burning temperature [ $^{\circ}\text{C}$ ]	Radiation brightness [ $\text{W}\cdot\text{m}^{-2}\cdot\text{sr}^{-1}$ ]
18	Sheet-like	1-1	0.0007	0.0597	1080.51	1912.11
		1-2	0.0008	0.0599	1151.93	1936.66
		1-3	0.0008	0.0624	1145.08	1765.86
		1-4	0.0008	0.0611	1136.83	1882.48
		1-5	0.0008	0.0597	1089.33	1900.24
		1-6	0.0008	0.0583	1145.38	1829.92
		Average	0.0008	0.0602 <sup>+3.7%</sup> <sub>-3.1%</sub>	1124.84 <sup>+2.4%</sup> <sub>-3.9%</sub>	1871.21 <sup>+3.5%</sup> <sub>-5.6%</sub>
	Column-like	2-1	0.0013	0.0505	1059.82	1678.62
		2-2	0.0012	0.0499	976.53	1581.23
		2-3	0.0012	0.0472	1078.50	1698.73
		2-4	0.0013	0.0470	1076.15	1684.36
		2-5	0.0012	0.0483	983.98	1598.44
		2-6	0.0012	0.0503	981.02	1623.21
		Average	0.0012	0.0489 <sup>+3.3%</sup> <sub>-3.8%</sub>	1026.00 <sup>+5.1%</sup> <sub>-4.8%</sub>	1644.10 <sup>+3.3%</sup> <sub>-3.8%</sub>
23	Sheet-like	3-1	0.0008	0.1257	1158.91	1948.70
		3-2	0.0008	0.1166	1151.34	1951.49
		3-3	0.0007	0.0941	1163.94	1944.66
		3-4	0.0008	0.1114	1147.21	1924.56
		3-5	0.0007	0.1102	1169.56	1973.65
		3-6	0.0008	0.1243	1157.42	1946.60
		Average	0.0008	0.1137 <sup>+10.5%</sup> <sub>-17.3%</sub>	1158.06 <sup>+1.0%</sup> <sub>-0.9%</sub>	1948.28 <sup>+1.3%</sup> <sub>-0.01%</sub>
	Column-like	4-1	0.0011	0.0971	1108.61	1944.30
		4-2	0.0012	0.0899	1194.09	2034.53
		4-3	0.0012	0.0862	1067.08	1735.93
		4-4	0.0012	0.0801	1071.75	1746.96
		4-5	0.0014	0.0738	1116.17	1827.97
		4-6	0.0012	0.0935	1108.13	1745.19
		Average	0.0012	0.0868 <sup>+11.9%</sup> <sub>-14.9%</sub>	1110.9 <sup>+7.5%</sup> <sub>-4.0%</sub>	1839.15 <sup>+10.6%</sup> <sub>-5.6%</sub>
30	Sheet-like	5-1	0.0008	0.1372	1191.58	2021.32
		5-2	0.0008	0.1384	1189.81	2025.74
		5-3	0.0009	0.1406	1177.01	1992.44
		5-4	0.0008	0.1390	1189.64	2014.68
		5-5	0.0008	0.1376	1176.35	2024.17
		5-6	0.0008	0.1387	1194.44	2020.63
		Average	0.0008	0.1386 <sup>+1.5%</sup> <sub>-1.0%</sub>	1186.47 <sup>+0.7%</sup> <sub>-0.9%</sub>	2016.50 <sup>+0.5%</sup> <sub>-1.2%</sub>
	Column-like	6-1	0.0012	0.1124	1162.15	1890.72
		6-2	0.0011	0.1099	1177.69	1996.19
		6-3	0.0011	0.1161	1148.16	1992.38
		6-4	0.0011	0.1133	1188.27	1875.92
		6-5	0.0011	0.1117	1175.31	1986.71
		6-6	0.0011	0.1142	1197.35	1975.26
		Average	0.0011	0.1129 <sup>+2.8%</sup> <sub>-2.7%</sub>	1174.82 <sup>+1.9%</sup> <sub>-2.3%</sub>	1952.865 <sup>+2.2%</sup> <sub>-3.9%</sub>

more heat released per unit time. Therefore, a larger diameter led to higher burning rate and higher burning temperature, thus to higher radiation brightness.

### 3.2 Differences in radiation brightness compared between sheet-like and column-like MTV infrared decoys

Radiation brightness was tested by the OPAG33 FTIR spectrometer, and the results were shown in Figure 4, 5 and Table 2.

As shown in Table 2, when the samples had the same diameter, column-like samples exhibited higher radiation brightness than sheet-like samples. The radiation brightness of the column-like samples was concentrated in near- and middle-infrared waves, at  $2.5-3.0\mu\text{m}/3.0-$

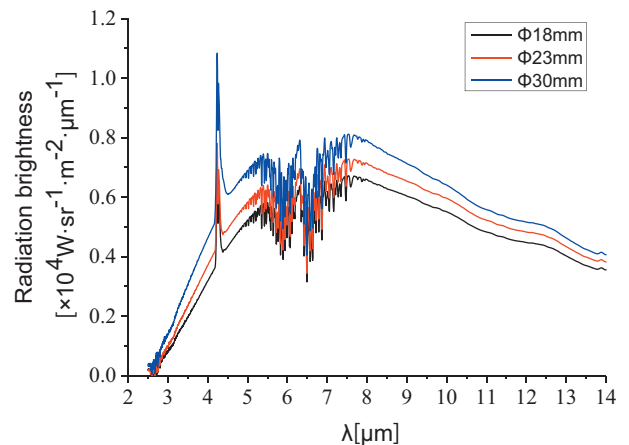


**Figure 4** Distribution of radiation brightness of sheet-like decoys

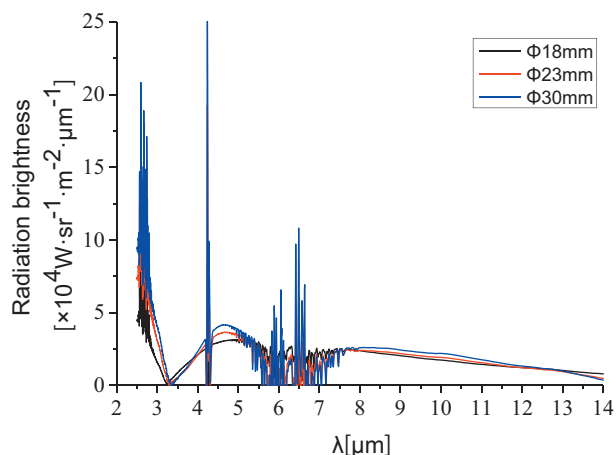


**Figure 5** Distribution of radiation brightness of column-like decoys

$5.0\mu\text{m} = 0.825 - 3.695$ . In comparison, the radiation brightness of the sheet-like samples was concentrated in middle- and far-infrared waves, at  $2.5 - 3.0\mu\text{m}/3.0 - 5.0\mu\text{m} = 0.116 - 0.164$ . The sheet-like samples had intense radiation peaks in  $4.24\mu\text{m}$ , while the column-like samples had intense radiation peaks in except  $4.24\mu\text{m}$  and  $2.60\mu\text{m}$ . This phenomenon is perhaps because there were a large number of reaction products, such as  $\text{MgF}_2$  ( $3.04 - 3.50\mu\text{m}$ ,  $9.97 - 13.77\mu\text{m}$ ),  $\text{CF}_4$  ( $7.82\mu\text{m}$ ),  $\text{CO}_2$  ( $4.17 - 4.48\mu\text{m}$ ),  $\text{CO}$  ( $4.60 - 4.78\mu\text{m}$ ) and  $\text{H}_2\text{O}$  ( $2.5 - 3.15\mu\text{m}$ ,  $4.67 - 8.13\mu\text{m}$ ). Furthermore, according to Wien's displacement law, the spectral will shift to the side of short waves because of the high burning temperature. After the absorption and scattering of the atmosphere, there are sharp picks in around  $2.5\mu\text{m}$  and  $4.25\mu\text{m}$ . The sheet-like samples have fewer compositions, so that there are fewer burning products, the radiation brightness in whole wave band is much smaller than column-like samples. The burning rate of sheet-like samples is larger, which may lead to the incomplete reaction of Mg and produce less  $\text{MgF}_2$ , so that the near-infrared radiation brightness is just  $0.036 - 0.069 \times 10^4 \text{W}\cdot\text{m}^{-2}\cdot\text{sr}^{-1}$ , the radiation brightness of sheet-like samples is concentrate in middle- and far-infrared. On the other hand, the column-like samples have much more compositions and the burning rate is smaller, the Mg may react with PTFE much easier and more completely, so that there're more  $\text{MgF}_2$ , which can generate intense radiation in near-infrared wave band.

Moreover, sheet-like samples show smaller radiation brightness at  $8.0 - 14.0\mu\text{m}$  than column-like samples

(Table 2), which is inconsistent with the results in Table 1. One possible reason is that the thermal imager detects the solid products above  $500^\circ\text{C}$ , while the spectrometer detects the gaseous products. Apparently, the speeds of heat exchange with the environment are different between solid products and gas products. Another reason is that sheet-like samples contain a smaller proportion of compositions and are more susceptible to the environment. As a result, the gas products measured by the spectrometer are at a relatively lower temperature, leading to lower far-infrared radiation brightness measured by the spectrometer.

Moreover, a larger sample diameter leads to higher radiation brightness, most likely because column-like samples and larger-diameter samples contain a large proportion of compositions and their burning produces more byproducts, which, in turn, leads to higher radiation brightness. Moreover, compared with column-like samples, the sheet-like samples are burnt more quickly, and the plume has too small power for combustion. As a result, a part of Mg without efficient oxidation passes through the burning zone, leading to the production of little energy<sup>15</sup>. The unreacted Mg may undergo oxidation with the outside air and consumes the oxygen in the air, and thus reduces the contents of highly-radiant  $\text{CO}_2$  and  $\text{H}_2\text{O}$  in the near and middle-infrared ranges in local areas. Accordingly, the contents of  $\text{CF}_4$ ,  $\text{MgF}$ ,  $\text{MgF}_2$  and  $\text{MgO}$  which are strongly radiant at middle- and far-infrared ranges are increased in these areas. Thus, sheet-like samples exhibit generally lower radiation brightness, which is concentrated in middle and far-infrared waves.

## 4. Conclusions

(1) Results from the thermal imager show that at the same diameter, the sheet-like MTV infrared decoys exhibit a more rapid burning rate, a higher combustion temperature, and higher far-infrared radiation brightness, when compared with column-like decoys. When physical forms are the same, a larger sample diameter is associated with a higher burning rate, a higher burning temperature, and larger far-infrared radiation brightness.

(2) Results from the FTIR spectrometer show that sheet-like decoys exhibit generally lower radiation brightness than column-like decoys. The spectral radiance of column-like samples is concentrated in near- and middle-infrared waves, while that of sheet-like samples is concentrated in middle- and far-infrared waves. When physical forms are

**Table 2** Spectral radiation brightness of samples.

Diameter [mm]	Physical form	Radiation brightness [ $\times 10^4 \text{W}\cdot\text{m}^{-2}\cdot\text{sr}^{-1}$ ]							
		2.5 - 3.0 $\mu\text{m}$		3.0 - 5.0 $\mu\text{m}$		8.0 - 14.0 $\mu\text{m}$		(2.5 - 3.0 $\mu\text{m})/(3.0 - 5.0 \mu\text{m})$	
		Mean	Max	Mean	Max	Mean	Max	Mean	Max
18	Sheet	0.036	0.084	0.284	0.721	0.526	0.659	0.125	0.116
	Column	4.095	10.277	1.573	3.155	1.654	2.393	2.604	1.257
23	Sheet	0.042	0.100	0.329	0.780	0.569	0.713	0.128	0.129
	Column	7.380	18.447	1.997	19.252	1.724	2.420	3.695	0.958
30	Sheet	0.069	0.142	0.421	1.083	0.615	0.790	0.164	0.131
	Column	8.581	20.820	2.394	25.227	1.907	2.611	3.584	0.825

the same, a larger diameter is associated with higher radiation brightness.

## References

- 1) C. L. Yeh, M. M. Mench, and S. K. Chan, *Int. J. Energ. Mater. Chem. Propul.*, 4, 465–475 (1997).
- 2) A. Peretz, *J. Spacecr. Rockets*, 21, 222–224 (1984).
- 3) E.C. Koch, *Propellants Explos. Pyrotech.*, 27, 262–266 (2002).
- 4) E. C. Koch, and Axel Dochnahl, *Propellants Explos. Pyrotech.*, 25, 37–40 (2000).
- 5) J. Callaway, US Patent 6,013,144, Washington DC, USA (2000).
- 6) L. A. Baldi, US Patent 6,193,814 B1, Washington DC, USA (2001).
- 7) A. K. Lay, US Patent 20,090,050,245 A1, USA (2009).
- 8) M. H. Chen, and G. H. Ma, *Laser & Infrared*, 38, 1008–1010 (2008).
- 9) M. H. Chen, Q. J. Jiao, and F. Chang, *Initiators & Pyrotechnics*, (3), 4–8 (2002).
- 10) J. B. Robert, “Field of view in introductory Fourier transform Infrared”, Academic Press (1972).
- 11) M. H. Chen, Q. J. Jiao, Y. Q. Wen, and B. Lu, *Laser & Infrared*, 35, 500–503 (2005).
- 12) N. Kubota and C. Serizawa, *J. Propul. Power*, 3, 303–307 (1987).
- 13) E. C. Koch, *Propellants Explos. Pyrotech.*, 27, 340–351 (2002).
- 14) E. C. Koch, “Metal-Fluorocarbon Based Energetic Materials”, John Wiley & Sons Press (2012).